Lamellar compact bone failure in tensile dynamic loading

Martine Pithioux — Patrick Chabrand

Laboratoire d'Aérodynamique et de Biomécanique du Mouvement
CNRS/Université de la méditerranée
163 av de luminy, Case Postale 918, 13288 Marseille Cedex 09
{pithioux, chabrand}@morille.univ-mrs.fr

ABSTRACT. *Shock Biomechanics is a research domain mainly devoted to the development of safety conditions during locomotion and also in accidentology, or sport practices. The objective of this study is to improve the knowledge of the biomechanical behaviour of bones to sudden tensile dynamic loading. Femur and tibia are often broken during a shock, but actually, bones behaviours are studied in quasi-static but the failure caused by dynamic loading has not drawn the attention of many authors. Many of the tissues which constitute the lower limb, such as cartilage, ligaments and bones are fibrous. The objective of this work is to finely analyse the failure of a lamellar fibrous compact bone caused by a shock. The originality of this work is to describe failure in terms of the loss of cohesion between fibres of lamellar bone in dynamic loading. This model permits us to investigate the role plays by various parameters which influence failure of bones. Among them, bone porosity was found to be the most significant. In parallel, failure profiles of bovine compact bones are analysed experimentally in dynamic. Results were found to be comparable with our numerical model.*

RÉSUMÉ. *La biomécanique du choc est un domaine de recherches principalement consacré à l'étude de la locomotion et à l'accidentologie, ou le sport pratique. L'objectif de cette étude est d'améliorer la connaissance du comportement biomécanique des os sous chargement dynamique. Le fémur et le tibia sont souvent cassés lors d'un choc, mais actuellement, le comportement des os est étudié en quasi statique et la rupture en dynamique est peu étudiée. Plusieurs tissus qui constituent le membre inférieur, tel que le cartilage, les ligaments et les os sont fibreux. L'objectif de ce travail est de décrire la rupture d'un os compact fibreux lamellaire provoqué lors d'un choc. Son originalité est de décrire la rupture en termes de perte de cohésion entre les fibres de l'os lamellaire sous sollicitations dynamiques. Ce modèle nous permet d'étudier les divers paramètres qui influencent la rupture des os compacts. Parmi eux, la porosité des os s'est avérée la plus significative. En parallèle, des profils de rupture des os compacts bovins sont analysés expérimentalement en dynamique. Les résultats sont comparables à notre modèle numérique.*

KEYWORDS: *structural approach, interactions between fibres, finite elements method, dynamics, Mohr Coulomb cohesive law, traction experiments.*

MOTS-CLÉS : *approche structurale, interactions entre les fibres, méthode éléments finis, dynamique, loi cohésive de Mohr Coulomb, expériences de traction.*

REEF – 14/2005. Biomechanics of impact, pages 445 to 461

1. Introduction

Bones injuries occur frequently in case of a shock and a better estimation and prevention may lie in the improvement of the biofidelity of the human numerical models. Biological materials such as bones are fibrous structures. If we analyse failure of such structures during a shock, they are exposed to dynamic tearing, damage and failure mechanisms which are induced by the fibrous structure. Quite a lot of research has been carried out on the mechanical behaviour of hard and soft tissues when submitted to quasi-static loadings, but damage and failure caused by dynamic loading has not drawn the attention of many authors (Aamodt *et al.*, 1997; Katsamanis F. *et al.*, 1990, Saha S., 1977). Various methods have been used (Hopkinson bar stress method and in vivo strain measurements) to characterize the human femoral cortical bone behavior but for a non-damaging range of loadings. Only (Saha S., 1977) tested compact bone samples under impact, for a velocity of 0.3 m/s. In our study, we analyze failure of bones under a velocity of 1m/s. A few authors have carried out experiments using micro-macro techniques. We can refer to the homogenisation method developed by (Crolet J.M. *et al.*, 1993), and the thermodynamic approach proposed by (Carter D.R. *et al.*, 1985). Other authors have focused their work on the study of the mechanical behaviour of bone microstructure (Bonfield W. et al. 1966; Bonfield W. *et al.*, 1966; Bonucci E., *et al.*, 1990; Currey J.D., 1970; Fung Y.C., 1993; Katz J.L., *et al.*, 1971; Piekarski K., 1970; Pithioux M. *et al.*, 2002; Sasaki N., *et al.*, 1996). These models have not however been used to study bone failure.

The objective of this work is to develop i) an experimental study which analyses failure of lamellar compact bone in dynamic and ii) a multiscale model based on the lamellar microstructure of compact bones subjected to a dynamic solicitation as far as failure. The originality of this study is double. First the sample used for experimentation has a geometry known and the structure is homogeneous. So an experimental material approach is developed and results of this experimental study can be compared with the numerical model. Second, we introduce a cohesive model where failure is introduce by a loss of cohesion between longitudinal and transversal joints fibres. So, we assume that fibres are considered to be the elementary structural components with the lowest failure characteristic. The cohesive composite material is constituted by elastic fibres. The behaviour of the joints between these fibres is described by unilateral contact, friction and cohesive laws (Jean M., 1995; 1999). We analyse the role play by the parameters of the model which can influence the failure behaviour. This led us to propose a phenomenological model of compact bones including these parameters.

2. Structure of lamellar compact bone

A general overview of the specific nature of the hierarchical structure (Figure 1) of bone is helpful in understanding why we wanted to develop this fibrous model.

The constitution and geometric structure of bones are highly complex (Evans F.G., *et al.,* 1967; Weiner S. *et al.,* 1992). The main deformation mechanisms can occur at four different levels:

– in the tropocollagen molecule and the microfibril (length = 2800 $\breve{A}$), elongation mechanisms set the molecule profile (Bonucci E., el al., 1990; Pithioux M., 2000; sasaki N., *et al.,* 1996). The authors (Comminou M., *et al.,* 1976; Piekarski K., 1973) have proposed mechanical models based on the waviness of the microfibrils. At this level, the microfibrils were found to be elastic (Gottesman T., *et al.,* 1980; Piekarski K., 1970; Piekarski K., 1973; Reilly D.T. *et al.,* 1975);

– in the fibrils (length = 10 μm to 100 μm), the arrangement of overlapping and gap regions has been described on the basis of the Hodge Petruska model (Hodge A., *et al.,* 1962; Sasaki N., *et al.,* 1996). The joints in the bone structure consist of a mineral hydroxyapatite component shown to exhibit elastoplastic behaviour (Gilmore R.S., *et al.,* 1982; Katz J.L., *et al.,* 1971; Katz J.L., 1979; Sasaki N., *et al.,* 1996);

– *The fibre* is a geometrical assembly of disjointed fibrils;

– The *fibre-lamella* assembly is made up of fibres which are all oriented in the alignment of the axis of the lamellae. The lamella is supposed like the biological unit base of the structure of compact bone. The lamellas are constituted of two components: an organic (collagen) and a mineral (hydroxyapatite) one.

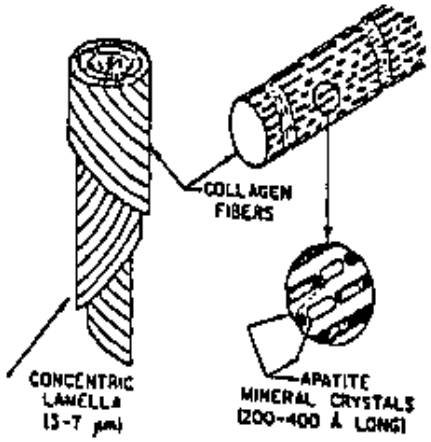

Figure 1. *Assembly of the different hierarchical levels in the lamella structure*

3. Dynamic experimental tensile method

Before study tensile failure of bone in dynamics, we analyse the structure of the femur using an X-ray scanner, type ND8000, Laboratoire de Mécanique et d'Acoustique. The samples were taken from 10 fresh bovine femoral bones.

Animals were from five to seven years old at the time of death. The bones were frozen prior to the experiments. The epiphyses were cut off so that we could concentrate our attention only on compact bone. Using the X-ray scanner, the density of the diaphyse was analyzed in ten sections cut 1 mm thick slices every 10 mm (PithiouxM., *et al.,* 2002). We found two types of sections. Type I sections where the radiological density was 900 CT (± 10 CT), and type II sections where the radiological density varied from 800 CT to 1100 CT. We then used an optical microscope to analyse the section structure more accurately. Type I samples had a lamellar structure, whereas type II samples had an osteonal structure. We chose to work on type I samples that were as homogeneous as possible in order to reduce the number of relevant parameters which explained failure process and to compare results with the numerical model. Finally, samples were cut in the anterior lateral and anterior medial parts. Bone shafts were taken and cut in the axial direction and marrow was removed from each part. Samples were then machined with a numerically controlled machine tool. The sample width was gradually reduced and shaped as shown in figure 2 to avoid the appearance of failure close to the extremities.

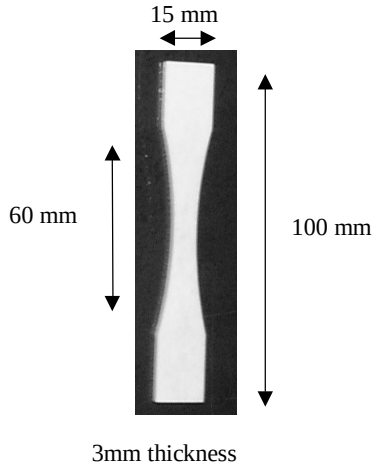

Figure 2. *Isolated sample*

Dynamic experiments

We designed a special device to perform dynamic tensile tests (velocity: 1m/s) (Figure 3) (Pithioux M., *et al.,* 2004). It was attached to a hydraulic jack fixed onto the upper traverse beam. The realised displacements, velocities, and accelerations were measured, with upper chuck jaw displacements and velocities being measured using a laser vibrometer. Displacement was obtained by interference measurements with an uncertainty of measurement of 1 %, whereas velocity was measured by the Doppler effect and acceleration by an accelerometer fixed onto the upper chuck jaw.

Force was measured by a triaxial piezoelectric sensor set on the lower chuck jaw, which measured forces in the tensile direction, with an uncertainty of measurement of 4.7 %, and in the shear plane. The hydraulic device was validated by carrying out tests on known materials. An initial displacement of 1/100 mm, that is to say a 0.016 % global strain, was prescribed in order to avoid dynamic effects due to the assembling of the system, especially the clearance. The sampling rate of the data acquisition was 32 kHz with tests lasting about 3 ms. This high sampling rate led us to use the laser vibrometer whose cut-off frequency was higher than the sampling rate. We studied plasticity of bone by hysteresis tests which were realised in imposing cycles every 0.1% of strain up to 0.5%. Moreover, we developed relaxation tests to observe viscous behaviour. In these experiments, displacement, equivalent to strain, was prescribed and the force variations, equivalent to stress variations, were measured. Finally, tensile tests up to failure were performed.

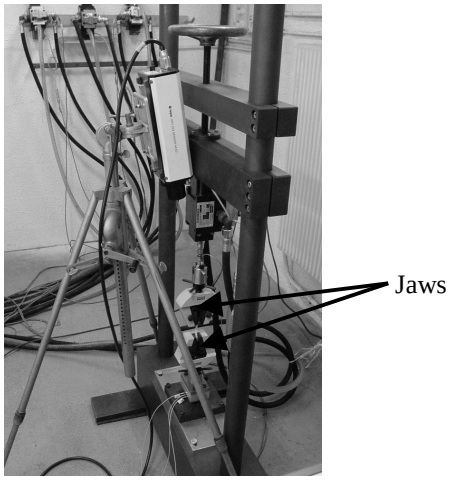

Figure 3. *Experimental device*

4. Fibrous model

Lamellar microstructure of compact bone is fibrous. In our model failure process is assumed to be caused by successive cohesive failure events occurring at different scales and aggregating so as to generate micro-voids or micro-cracks, that well up into aggregates generating voids or cracks on a larger scale. There remains the possibility of exploring an assembly of model-fibres linked together with appropriately distributed cohesive forces. The following fibrous model (cf. Figure 4a) consists of an assembly of fibres, in which joints are formed longitudinally and transversally between the fibres (cf. Figures 4b). In the fibrous structure the ability to bear tensile stress results from two classes of cohesive forces. These are: (i) the fore end of each fibre on the aft end of the previous fibre (head to

tail or longitudinal cohesive force called f_1); and (ii) the flanks of neighbouring fibres (flank to flank or transversal cohesive force called f_2). The principal component of the head to tail forces is tensile, while the principal component of the flank to flank forces is a shear force. In this study, tensile tests in the direction of the fibres were taken into account. The constitutive laws were therefore developed from a fibrous model subjected to tensile applied in the direction of the fibre axes (this model could be a lamellar structure). Because of the dynamic kinematics involved, damage was assumed to be preponderant, and viscosity was neglected.

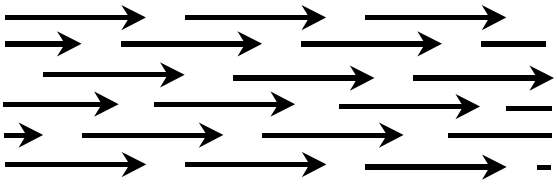

Figure 4a. *Fibrous assembly*

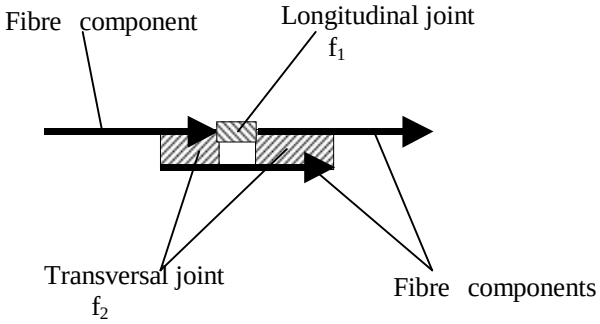

Figure 4b. *Example of unit fibrous assembly projected onto a two dimensional plane. f_1 is the cohesive coefficient of the shear between two fibre layers. f_2 is the tensile cohesive coefficient for the fibres cohesion on the same layer*

4.1. *Joint model*

In this model, interactions between fibres are described using unilateral contact conditions and Coulomb's friction coefficient. Let n be the normal unit vector to the contact interface. The normal relative displacement between two contacting fibres is then defined by q_N = q.n. decomposing the contact force vector R into the normal (R_N) and tangential (R_T) components gives: $R = R_N.n + R_T$.

In the cohesive model, the unilateral constraints (Signorini conditions) are written as follows [1]:

$$q_N \geq 0,\ R_N + l \geq 0,\ (q_N,\ R_N + l) = 0 \qquad [1]$$

where l is the longitudinal cohesive threshold.

The joint model characterises a cohesive Mohr Coulomb law (cf. Figure 5) which corresponds to a translation of the Coulomb cone.

The corresponding law for friction with adhesion in terms of the threshold μl is given by relations 2.a, 2.b and 2.c:

$$U_T = 0 \quad \Rightarrow R_T \in]-\mu (R_N+l)\ ;\ \mu (R_N+l)[\qquad [2.a]$$

$$U_T < 0 \quad \Rightarrow R_T = -\mu (R_N+l) \qquad [2.b]$$

$$U_T > 0 \quad \Rightarrow R_T = \mu (R_N+l) \qquad [2.c]$$

where μl is the transversal cohesive breakdown threshold.

This cohesive law can result in two possible situations occurring at the contact interfaces:

– if (R_N, R_T) lies inside the Coulomb cone (point A in Figure 5 for example) the fibres stick together and there is no relative displacement;

– if (R_N, R_T) lies on the cone boundary (point C for example in Figure 5), the cohesive status is lost and friction occurs between the fibres, which corresponds to local damage (i. e. the joints between the fibre components are broken)

The static sliding coefficient μ is defined by $\mu = tg\alpha = L/l = f_2/f_1$ (cf. Figure 5).

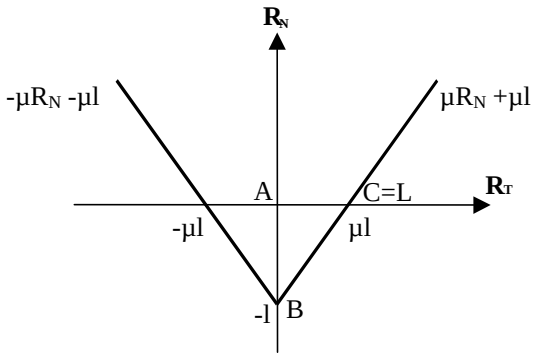

Figure 5. *Mohr Coulomb cohesive law*

The cohesive thresholds differ between longitudinal (f_1) and transversal (f_2) joints and are related to maximal head to tail and flank to flank cohesive forces.

When the joints are broken, the classical unilateral Signorini conditions [3] involving Coulomb's friction [4.a, 4.b and 4.c) give:

$q_N \geq 0 \; ; \; R_N \geq 0; \; (q_N, R_N) = 0$ [3]

$U_T = 0 \quad \Rightarrow R_T \in]-\mu_f R_N \; ; \; \mu_f R_N[$ [4.a]

$U_T < 0 \quad \Rightarrow R_T = -\mu_f R_N$ [4.b]

$U_T > 0 \quad \Rightarrow R_T = \mu_f R_N$ [4.c]

where U_T is the sliding celerity and μ_f is the Coulomb's friction coefficient.

In order to introduce local defects into the structure, we applied a stochastic process to choose the cohesive thresholds for the model.

4.2. *Dynamic equation and boundary conditions*

Assuming the fibres exhibit elastic behaviour, the principle of virtual power was used to obtain the dynamic equation, the discrete form of which leads to the following system:

$$M\ddot{q} + Kq = F + r \qquad [5]$$

where M is the mass matrix, K the rigidity matrix, $\ddot{q}$ (resp q) the nodal acceleration vector (resp displacement), F is the external force vector and r the contact force vector.

The boundary conditions must account for the behaviour of the surrounding material. On the lateral sides, the displacements were taken to be zero for all left-hand side nodes (Ux=0). Though several different boundary conditions may be applied to the upper and lower sides, they were chosen to specify $\sigma_{yy} = 0$ and identical displacements in the y displacements of the upper and lower sides ($q_y^{sup} = q_y^{inf}$). These conditions are characteristic of periodic boundary conditions describing the effect of the material surrounding the sample in a tensile experiment. For all right-hand side nodes, only displacements along the x axis are specified:

$$q_x = \dot{\varepsilon}_{xx}(L.t) \qquad [6]$$

In [6] $\dot{\varepsilon}_{XX}$ is the specified strain rate, L is the length of the fibre and t the time. The boundary conditions chosen limit swelling effects but the Poisson effect is free to act on the structure.

To reduce side effects, we have introduced a new set of variables in which the new variable u is defined by:

$$q(x,t) = u(x,t) + t\left[\dot{A}\right](x) \qquad [7]$$

with $\dot{A} = \begin{bmatrix} \dot{\varepsilon}_{xx} & 0 \\ 0 & \dot{\varepsilon}_{yy} \end{bmatrix}$

where $\dot{\varepsilon}_{XX}$ and $\dot{\varepsilon}_{YY}$ are the constant specified strain rate.

The discrete form of the dynamic equation can then be written as:

$$M\ddot{u} + Ku = -K\dot{A}t + F + r \qquad [8]$$

The boundary conditions become:

σ_{yy}=0 with similar displacement of the upper and lower sides ($u_y^{sup} = u_y^{inf}$).

The advantage of such a variable change is that it gives a "smooth numerical" problem.

When a transformation of the discrete time domain is performed, an elementary subinterval $]t_l, t_{l+1}]$, of length h is considered. The principal consideration developed in this transformation is that discrete variables do not necessarily have to be defined at a specific time within this interval. In any case, the impact times are usually unknown, or it can be difficult or costly to approximate or isolate when simultaneous contacts occur.

Let t_l be the time at the previous increment and t_{l+1} the time of the current load in progress. $\dot{q}(I)$ denotes an approximation of $\dot{q}(t_I)$ and $\dot{q}(I+1)$ an approximation of $\dot{q}(t_{I+1})$. We use the same notation for the other parameters.

The discrete dynamic equation is solved using an implicit Euler method with the schema:

$$\begin{cases} h\ddot{q}(I+1) = \dot{q}(I+1) - \dot{q}(I) \\ q(I+1) = q(t_I) + h(\dot{q}(I+1) - \dot{q}(I)) + h\dot{q}(I) \end{cases} \qquad [9]$$

At time t_{l+1}, the equation [5] can be rewritten as follows:

$$\begin{cases} \dot{q}(I+1) - \dot{q}(I) = w[-hK(q(I) + h\dot{q}(I)) + hF(I+1) + hr(I+1)] \\ with\ w = \left(M + h^2K\right)^{-1} \end{cases} \qquad [10]$$

The "Non Smooth Contact Dynamic Method" presented in (Jean M., 1999) is used to deal with the frictional contact problem.

4.3. *Finite element modelling*

To analyse the development of failure in structural bone tissue, a representative volume was obtained by assembling 21 fibres longitudinally in 30 successive layers. With the cohesive model, each fibre was represented by a 2D elastic model-fibre. Each model-fibre was composed of eight T3-triangle linear finite elements. Cohesive frictional contact forces were exerted between model-fibres and, for numerical purposes, were assumed to be concentrated at specific midpoints.

Several authors (Bonfield W., *et al.*, 1966; Currey J.D., 1970; Fung Y.C., 1993; Katz J.L., 1979; Piekarski K., 1970; Piekarski K., 1973; Reilly D.T. *et al.*, 1975; Sasaki N., *et al.*, 1996) have measured and analysed the mechanical properties of collagen and hydroxyapatite (Young's modulus, Poisson's ratio and density). In accordance with these works, the fibres were assumed to be elastic with a Young's modulus E between 11 GPa and 16 GPa. The Young's modulus considered was an average of the collagen and hydroxyapatite modulus because in our model-fibre the mineral and collagen components were considered as a single equivalent material. The density d of the fibres was 2 10^3Kg/m^3 and the Poisson ratio ν was 0.33. The cohesive forces of the joints correspond to the plasticity values of the hydroxyapatite mineral.

f_1 is taken to be the cohesive head-tail stress for each layer and f_2 the cohesive shearing stress for each layer interface (Figure 4.b). In order to compare different responses obtained with a number of values of the ratio f_1/f_2 with a given global failure threshold, the resulting force f_{res}, was defined from:

$$f_{res} = (N-2)\, f_1 + 2\, f_{\partial 1} + (N-1)\, f_2 \qquad [11]$$

with $f_{\partial 1}$ the head tail force of the boundary fibres and N the number of layers

For the above relations, it was assumed that the boundary fibres are subjected to shear cohesive forces exerted by the neighbouring material equal to f_2. For the sake of simplicity and numerical processing, this force was included in the head tail force of the boundary fibres $f_{\partial 1}$ so that $f_{\partial 1} = f_1 + f_2$.

We obtain:

$$f_{res} = N\, f_1 + (N+1)\, f_2 \qquad [12]$$

Considering the height l and the length L of the fibrous structure (a unit value being assumed for thickness), the above formula can be written:

$$\frac{f_{res}}{Nl} = \frac{f_1}{l} + \frac{1}{2}\frac{N+1}{N}\frac{f_2}{L/2}\frac{L}{l} \qquad [13]$$

Equation [11] can be rewritten, introducing $\sum_{res}$, the equivalent tensile stress, $\sigma_1 = \frac{f_1}{l}$, the head tail cohesive stress and $\sigma_2 = \frac{f_2}{L/2}$, the equivalent shear cohesive flank-flank stress:

$$\sum_{res} = \sigma_1 + \frac{1}{2}\left(1 + \frac{1}{N}\right)\frac{L}{l}\sigma_2 \qquad [14]$$

Since f_1 and f_2 cannot exceed the maximum values of the cohesive threshold, the above formula [14] shows clearly that the stress-strain response curve depends on the f_1/f_2 ratio. If threshold values are measured as stresses, the ratio σ_1/σ_2 becomes a significant parameter together with the aspect ratio L/l.

5. Results

Since we modelled dynamic traction experiments, the deformation mechanisms had a traction wave effect which was reflected on the left-hand side where zero displacement was specified. The plastic deformations observed in joints may have resulted from these effects.

5.1. *Comparison between the numerical model and experimental results*

The objective of this work was to show how a cohesive model can be used to analyse macroscopic failure of bones. Experimentally, hysteresis tests showed that plasticity could be disregarded when describing bone behaviour. At the end of the cycle, there was no residual plastic strain (Figure 6a). In addition, the facies failure (Figure 7) confirmed that compact bone is a brittle material as no plastic strain was observed. Relaxation tests show that only an elastic return was observed after the sample was placed under tension (Figure 6b).

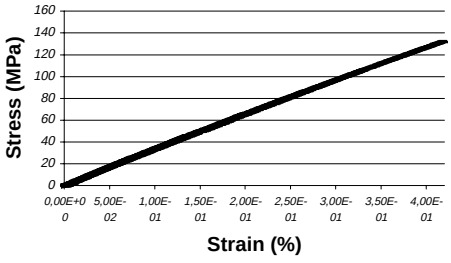

Figure 6a. *Hysteresis at 0.5% of strain*

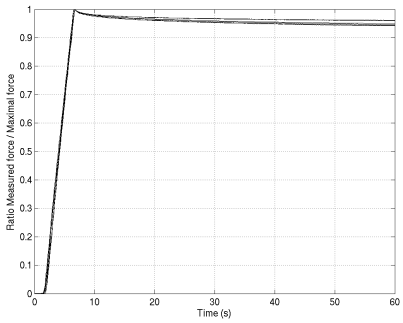

Figure 6b. *Compact bone relaxation according to time*

In conclusion, the tests carried out, justified the use of an elastic model for the compact bone in the range of the considered loading. Moreover, the plotted curves using the results of the numerical model showed a brittle elastic behaviour (Figures 9, 10 and 11).

The failure profile obtained in the experimental study is the same for all the samples which represents an Y form (Figure 7). In the model, failure does not occur as a result of the fibres breaking, but rather because they lose their structural stability in an avalanche process of cohesive failure. Cohesive failure of a few joints triggering a step by step failure process in the neighbouring vicinity. Longitudinally and transversally connected joints were also damaged and the structure was broken in only a few steps (Figure 8). Qualitatively, the experimental and computational results were quite similar (Figures 7, 8). Quantitatively, a study taking into account scale effects and dispersion between one bone to another is in progress.

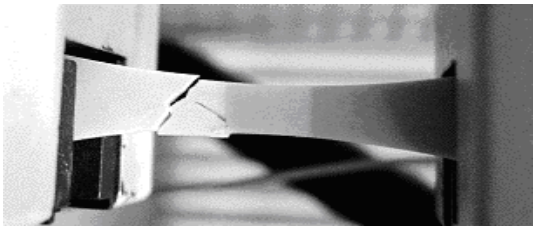

Figure 7. *Failure profile obtained with the experimental device. Sample has a lamellar*

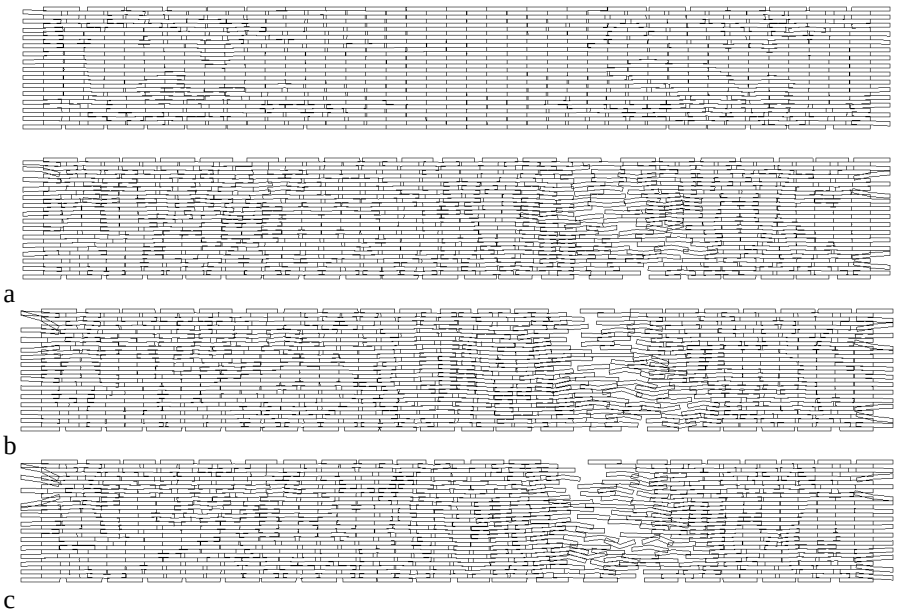

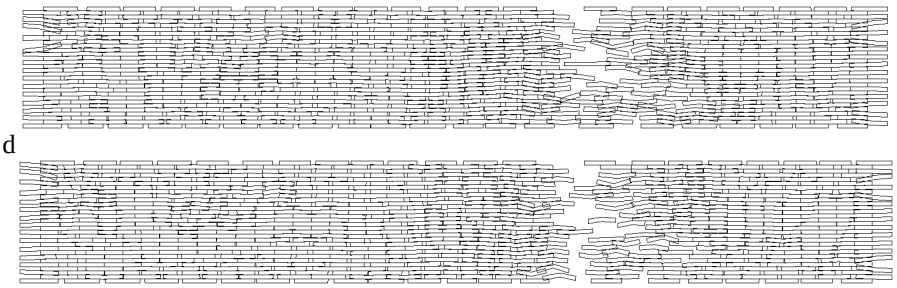

d

e

Figure 8. *Numerical results obtained when the fibres are assumed to be oriented at 0° with respect to the longitudinal axis. (a) t=0.013µs ; (b) t=0.0135µs ; (c) t=0.014µs ; (d) t=0.0145µs (e) t=0.015µs*

5.2. *Effect of model parameters*

In order to introduce local defects into the structure, different parameters model are studied. These parameters have no influence on the failure profile (Y form) of the samples but have an influence on the failure force values.

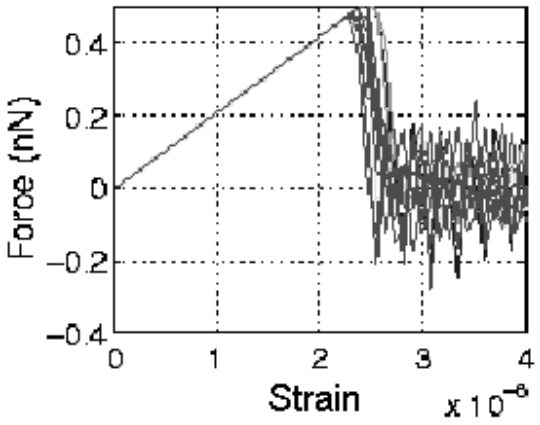

Figure 9. *Strain-force curve with randomised thresholds*

5.2.1. *Effect of local defects*

First, we studied the influence of the longitudinal traction thresholds (f_1) values and transversal shearing thresholds (f_2) values using a random method. The force-strain curves showed that this parameter (Figure 9) has no effect on the value of the failure force.

Second, the length of the interval within which the longitudinal traction thresholds (f_1) and transversal shearing thresholds (f_2) varied (it represents the scattering parameter). The scattering parameter influenced failure: structure fractures occurred more rapidly with longer intervals (Figure 10).

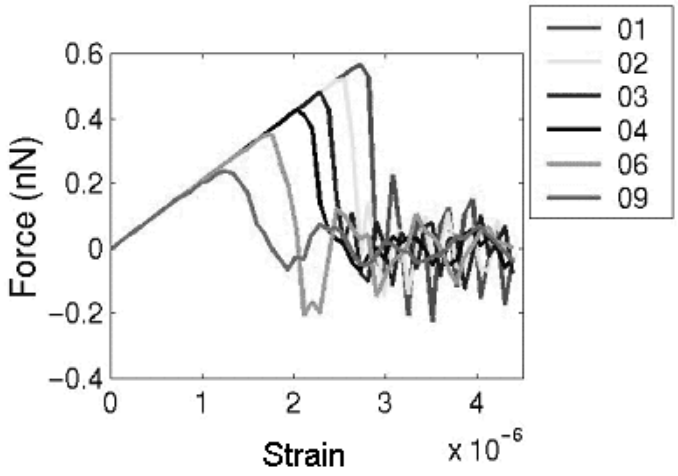

Figure 10. *Effects of scattering on the force deformation curve. The scattering parameter was more important for 01 than for 02 and for 02 than for 03.... The interval within which the longitudinal traction thresholds (f_1) and transversal shearing thresholds (f_2) is three times more longer for 01 than for 09*

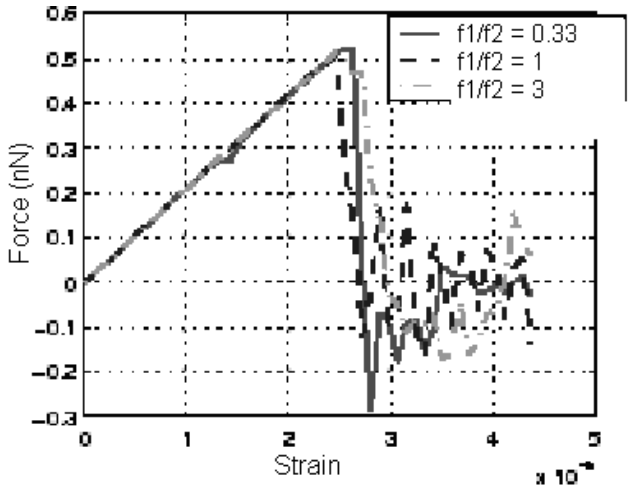

Figure 11. *Effect of the parameter f_1/f_2 when fibres are at 0° in comparison with the longitudinal axis*

5.2.2. *Effect of the ratio f_1/f_2*

Different assemblies of model-fibres, linked together with appropriately chosen cohesive forces, were then explored. The fibrous structure of the model was considered and the ability to bear tensile stress was found to be due to two classes of cohesive forces: forces exerted by the fore end of a fibre on the aft end of the proceeding fibre (f_1); forces exerted flank-to-flank between neighbouring fibres (f_2). In the context of tensile tests, f_1 forces were mainly tensile forces while f_2 forces were mainly shearing forces; the ratio f_1/f_2 was thus a significant mechanical parameter. We observed that the ratio f_1/f_2 had no effect on the failure force of the structure when fibres were oriented at 0° (lamellar structure) in comparison with the longitudinal axis of the bone (Figure 11).

6. Constitutive laws

From the previous results, we found that when we consider a lamellar structure of bone, only the scattering parameter plays an important role in the failure process. From, these results, we can study the evolution of the failure strain with respect to the scattering parameter. Experimental and numerical results showed that bone behaviour is brittle. We used a least squares resolution method to find representative laws of compact bones at failure:

The phenomenological model found is:

$$\sigma = E\varepsilon \text{ if } \varepsilon \leq \varepsilon_{ult} \quad [15]$$

$$\sigma = 0 \text{ if } \varepsilon \succ \varepsilon_{ult} \quad [16]$$

with $\varepsilon_{ult} = \varepsilon_0 \cdot d + \varepsilon_1$

d is the scattering parameter. $\varepsilon_0 = 1{,}8\ 10^{-6}$ and $\varepsilon_1 = 2{,}8\ 10^{-6}$

7. Discussion and conclusion

To summarise, in this paper, we propose a new method for investigating bone failure, following on from the development of earlier models of cortical bones. We develop an experimental study to characterize the material properties and behaviour instead of the one of the bone structure and to analyse failure in dynamic. Such experimental tests allowed us to compare numerical and experimental results. In our numerical model, bones are described as fibrous structures in which deformation occurs in the fibrous elements and damage results from the failure of joints between the fibres. A finite element model is used to describe the behaviour of this structure, based on cohesive laws as applied to joint modelling. With this model, we established how parameters such as scattering can strongly affect failure force value. The cohesive model gives a physical description of the damage resulting from joint

cohesive failure processes. The scattering parameter can be used to control the damage occurrence and its development. The physical meaning of the scattering parameter can be associated with the porosity of the material. This parameter is relevant for studying the failure at various level of the structure. Thus with this approach, the internal value of a microscopic and therefore macroscopic phenomenological model dealing with the physics of the damage processes can be defined.

Qualitatively, numerical results are in complete agreement with those obtained experimentally in dynamic for the lamellar structure of bone. This constitutes a first step towards describing a structural failure model in which damage occurs as the result of cohesive failure between longitudinal and transversal joints.

Our numerical model characterises a representative elementary volume of a macroscopic lamellar bone. Then a micro-macro assembly is needed for studying bones with lamellar structure. Moreover, the numerical model was developed considering the various orientations of the fibres in the haversian structure. Indeed, the lamella-osteonal assembly is made up of fibres which are oriented longitudinally, transversally and obliquely, *i.e.* forming angles of 0°, 45° and 90° with the longitudinal axis of the structure.

8. References

Aamodt A, Lund-Larsen J, Eine J, Andersen E, Benum P, Schnell Husby O., "In vivo measurements show tensile axial strain in the proximal lateral aspect of the human femur", *Journal of Orthopeadic Research*, 1997, 15, 927-931.

Bonfield W., Li, C.H., "Deformation and fracture of bone", *Journal of applied Physical*, 37, 2, 1966, 869-875.

Bonucci E., Motta, P.M., "Collagen mineralization: Aspects of structural relationship between collagen and the apatic crystallites", *Ultrastructure of Skeletal Tissues*, Kluwer Academic Publisher, 1990, 41-62.

Carter D.R., Caler, W.E., "A cumulative Damage Model for Bone Fracture", *Journal of Orthopeadic Research*, 3, 1985, 84-90.

Comminou M., Yannas, I., "Dependence of stress-strain nonlinearity of connective tissues on the geometry of collagen fibers", *Journal of Biomechanics*, 9, 1976, 427-433.

Crolet J.M., Aoubiza, B., Meunier, A., "Compact Bone: Numerical Simulation of Mechanical Characteristics", *Journal of. Biomechanics*, 26, 6, 1993, 677-687.

Currey J.D., "The Mechanical Properties of Bone", *Clin Orthop Related research*, 73, 1970, 210-231.

Evans F.G., Bang, S., "Difference and relationships between the physical property and the microscopic structure of human femoral, tibial and fibular cortical bone", *American Journal of Anatomy*, 120, 1967, 79-88.

Fung Y.C., *Biomechanics. Mechanical properties of living tissues,* Springer-Verlag, 1993.

Gilmore, R.S., Katz, J.L., "Elastic properties of apatites", *Journal of Materials Science*, 17, 1982, 1131-1141.

Gottesman T., Hashin, Z., "Analysis of viscoelastic behaviour of Bones on the basis of microstructure", *Journal of Biomechanics*, 13, 1980, 89-96.

Hodge A., Petruska, J., *Electron microscopy*, In Academic Press, New York, 1962.

Jean M., "Frictional contact in rigid or deformable bodies: numerical simulation of geomaterials", A. P. S. Salvaduai J. M. Boulon, *Elsevier Science Publisher*, Amsterdam, 1995, 463-486.

Jean M., "The non Smooth Contact Dynamic method", *Comput. Methods Appl. Mech. Engrg*, editors Martins, Klarbring, Elsevier, 177, 1999, 235-257.

Katsamanis F, Raftopoulos DD, "Determination of mechanical properties of human femoral cortical bone by the hopkinson bar stress technique", *J. Biomechanics*, 23, 1990, 1173-1184.

Katz J.L., Ukraincik K., "On the anisotropic elastic properties of hydroxyapatite", *Journal of Biomechanics*, 4, 1971, 221-227.

Katz J.L., "The structure and biomechanics of bone. Mechanical Properties of Biological Materials", *Cambridge University Press*, Cambridge, 34,. 1979, 137-168.

Piekarski K., "Fracture of bone", *Journal of applied physics*, 41, 1, 1970, 215-223.

Piekarski K., "Analysis of bone as a composite material", *Journal Engineering Science*, 11, 1973, 557-565.

Pithioux M., Lois de comportement et modèles de rupture des os longs, Thèse Université Aix Marseille II (2000)

Pithioux M., Chabrand P., Mazerolle F., "Statistical failure model of bones", *Journal of Mechanics in Medecine and Biology*, vol 2, n° 1, 2002, p. 19-27.

Pithioux M., Subit D., Chabrand P., "Compact bones failure models in quasi-static and dynamic solicitations", *Medical Engineering & Physics*, vol 26, 2004, p. 647-653.

Reilly D.T., Burstein, A.H., "The elastic and ultimate properties of compact bone tissue", *Journal of. Biomechanics*, 8, 10, 1975, 393-405.

Saha S, Hayes WC., "Relations between tensile impact properties and microstructure of compact bone", *Calcif. Tissue Res*, 1977, 24: 65-72.

Sasaki N., Odajima S., "Strain-Stress curve and Young's modulus of a collagen molecule as determined by the X-ray diffraction technique", *Journal of Biomechanics*, 29, 5, 1996, 655-658.

Sasaki N., Odajima, S., "Elongation mechanism of collagen fibrils and force strain relations of tendon at each level of structural hierarchy", *Journal of Biomechanics*, 29, 9, 1996, 1131-1136.

Weiner S., Traub, W., "Bone structure: from Angstroms to microns", *The Federation of American Societies for Experimental Biology Journal*, 6, 1992, 879-885.